Frustrated mixed-spin chains: Three-site interactions and flat-band magnons

S. Seyedi,[1,*] F. Heydarinasab,[2,*] and J. Abouie[1,†]

[1]*Department of Physics, Institute for Advanced Studies in Basic Sciences (IASBS), Zanjan 45137-66731, Iran*

[2]*Department of Physics, Faculty of Science, University of Sistan and Baluchestan, Zahedan, Iran*

(Received 16 December 2021; revised 16 August 2022; accepted 2 September 2022; published 14 September 2022)

We investigate the ground-state phase diagram of frustrated mixed-spin (1, 1/2) chains with three-site four-spin interactions employing different approaches, such as cluster mean field theory, cluster variational method, and spin-wave theory. The interplay of next-nearest-neighbor and three-site interactions leads to a plethora of magnetic and nonmagnetic phases in the ground-state phase diagram. We show that aside from the ferromagnetic and Neel orders, the ground state possesses a magnetic phase in which magnon excitations are dispersionless. The emergence of flat-band magnons is a consequence of the inhomogeneity of our frustrated mixed-spin chains and does not occur in similar uniform spin chains. We also demonstrate that the presence of three-site interaction gives rise to various nonmagnetic phases, such as antiferroquadrupole order and quantum spin-liquid phase.

DOI: 10.1103/PhysRevB.106.104412

I. INTRODUCTION

Quantum spin models are building blocks of condensed-matter physics and quantum information theory. The starting point for the study of quantum magnetic systems is often spin models with pairwise exchange interactions, but in beyond-Heisenberg systems, such as high-T_C superconductors [1], spin-liquids (SLs) [2], 1D magnetic material $CsMn_xMg_{1-x}Br_3$ [3], magnetic molecules [4,5], complex salts [6,7], and nuclear magnetism of solid ^{3}He [8,9], to reach results consistent with experiments, more realistic spin models with higher-order interactions should be considered [10–21]. One of the most common extensions is biquadratic interaction in $S \geqslant 1$ spin systems [22–26], which gives rise to different dimer and Haldane phases [26–29]. Multisite interactions are another proposal in amendment of the Heisenberg model in magnetic materials [5,8,12,15,30–35], which appear in fourth-order expansion of the two-orbital Hubbard model at half filling [32,36–38]. Recently, Hoffmann and Blügel demonstrated that multiorbital Hubbard models are effectively mapped onto a spin model with three-site four-spin interactions [39]. The three-site four-spin [19,34,35,39] and four-site four-spin [40] interactions are crucial in deriving the unusual up-up-down-down ground state of iron-based magnetic materials. Recently, much attention has been devoted to the study of the effects of three-site interactions on the ground-state phase diagram of spin-S Heisenberg models [32,41–46]. However, mixed-spin systems with beyond-Heisenberg models are rarely studied. Mixed-spin models are a special class in spin systems in which their universality class is completely different from uniform spin models [47–54]. Recently, it has been shown that the ground states of $J_1 - J_3$ ferrimagnetic spin-(1,1/2) chains, with J_1 and J_3 being nearest neighbor (NN) and three-site interactions, show nematic and quantum SL phases [55–58]. The focus of the previous studies was to investigate the effects of three-site interactions on the ground-state phase diagram of the standard mixed-spin systems with NN interactions. In this paper, in addition to the NN and three-site interactions, we also consider next nearest neighbor (NNN) (J_2) interaction, and reveal the combined effects of the NN, NNN, and three-site interactions on the ground-state properties of $J_1 - J_2 - J_3$ mixed-spin chains. We demonstrate that the interplay of the NNN and three-site interactions gives rise to interesting phases not seen in $J_1 - J_3$ and $J_1 - J_2$ models. By employing different approaches such as cluster mean field (CMF) theory, cluster variational method (CVM), and spin wave theory (SWT), we examine the ground-state phase diagram of $J_1 - J_2 - J_3$ mixed-spin (1,1/2) chains with beyond-Heisenberg Hamiltonians and show that, aside from the ferromagnetic (F) and Neel (N) orders, there is a magnetic up-up-down-down phase in which all magnon excitations are dispersionless. The emergence of flat-band magnons is a consequence of the inhomogeneity of our mixed-spin chains, not seen in similar uniform spin chains. We also demonstrate that different nonmagnetic orders such as antiferroquadrupole (AFQ) order and quantum SL phase appear in the ground-state phase diagram.

This paper is organized as follows. In Sec. II, we introduce our model and investigated the ground-state properties of a finite chain. In Sec. III, we present the classical phase diagram of the system and show that, in addition to the F and N orders, different highly degenerate phases also emerge in the phase diagram. In Sec. IV, we study the effects of quantum fluctuations by means of SWT and obtain the ground-state phases as well as magnon excitations. The results of cluster mean field theory (CMFT) and CVM are presented in Secs. V and VI. Finally, we summarize our results in Sec. VII.

II. MIXED-SPIN CHAINS WITH THREE-SITE EXCHANGE INTERACTIONS

Let us consider an alternating mixed-spin chain with spins S and T, described by the following

*These authors contributed equally to this work.
†jahan@iasbs.ac.ir

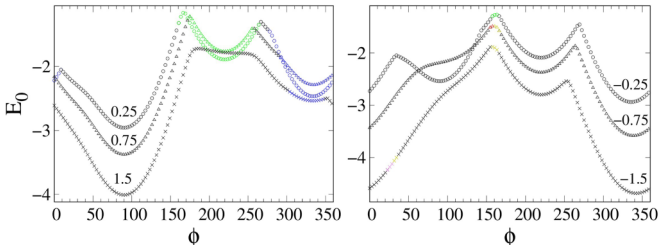

FIG. 1. The ground-state energy of a finite chain with $N = 4$ spins, versus ϕ, for different positive (left) and negative (right) values of three-site interaction. The green, blue, and black colors show, respectively, the ground states with ferromagnetic, Neel, and antiferroquadrupole orders. The yellow, purple, and red show, respectively, the degenerate ground states D1, D2, and D3, defined in Table I.

Hamiltonian:

$$H = \sum_{i=0}^{N} \big(J_1(\vec{S}_{2i}\cdot\vec{T}_{2i+1} + \vec{T}_{2i+1}\cdot\vec{S}_{2i+2}) + J_2^S\vec{S}_{2i}\cdot\vec{S}_{2i+2} + J_2^T\vec{T}_{2i+1}\cdot\vec{T}_{2i+3} + J_3^T[(\vec{S}_{2i}\cdot\vec{T}_{2i+1})(\vec{T}_{2i+1}\cdot\vec{S}_{2i+2}) + \text{H.c.}] + J_3^S[(\vec{T}_{2i-1}\cdot\vec{S}_{2i})(\vec{S}_{2i}\cdot\vec{T}_{2i+1}) + \text{H.c.}]\big), \quad (1)$$

where the summation runs over unit cells, and J_1, $J_2^{S,T}$, and $J_3^{S,T}$ refer to the NN, NNN, and three-site interactions, respectively. In the mixed-spin ($T = 1$, $S = 1/2$) chains, the three-site interactions J_3^S are reduced to the NNN interactions between T spins, and therefore we can set $J_3^S = 0$ without loss of generality. In the rest of the paper, we set $J_1 = J\cos\phi$, $J_2^S = J_2^T = J_2 = J\sin\phi$, and $J_3^T = J_3$.

Before examining the ground-state phase diagram of the Hamiltonian Eq. (1), it is insightful to investigate the ground-state properties of a finite chain. We obtained the energy spectrum of a chain of $N = 4$ spins ($S_1 - T_2 - S_3 - T_4$) for different values of exchange parameters, and plotted in Fig. 1 the ground-state energy versus the angle ϕ for different positive and negative values of J_3. The changes in the behavior of the ground-state energy are often due to level crossings in the energy spectrum which indicate ground-state phase transitions within the system. To classify the ground state of the system, we examine the behavior of the expectation values of S_i^α and T_i^α with $\alpha = x, y, z$. As illustrated by different colors (see Fig. 1), the ground state can have different magnetic and nonmagnetic orders. In the regions with green, blue, and black colors, the ground state has, respectively, F, N, and AFQ orders [see Eq. (14) for the definition], and in the narrow regions with yellow, purple, and red colors (see Fig. 1, right) the ground states are, respectively, the doubly degenerate D1, D2, and D3 states defined below. In the AFQ phase, the ground state is written in terms of the product states as follows:

$$|\text{AFQ}\rangle = \sum_{i_1,\ldots,i_4} c_{i_1,\ldots,i_4}(1 - \text{sgn}(J_3)\mathcal{S})|i_1,\ldots,i_4\rangle, \quad (2)$$

where $|i_1,\ldots,i_4\rangle$ is a product state (the eigenvectors of S^z_{total}) with i_n being the ith state at site n, the coefficients $c_{i_1,\ldots,i_4}$ depend on the exchange parameters, and $\mathcal{S} = \Pi_{n=1}^4\mathcal{S}_n$, with $\mathcal{S}_n$ being a spin-flip operator acting as

$$\mathcal{S}_n|\pm 1/2_n\rangle = |\mp 1/2_n\rangle, \mathcal{S}_n|\pm 1_n(0_n)\rangle = |\mp 1_n(0_n)\rangle. \quad (3)$$

In this $|\text{AFQ}\rangle$ state, all the expectation values, $\langle S_i^\alpha\rangle$ and $\langle T_i^\alpha\rangle$, are zero, and there is no magnetic order in the system. In the degenerate phases, the ground state is doubly degenerate and can be written as

$$|Dj\rangle = \sum_{i_1,\ldots,i_4} c_{i_1,\ldots,i_4}|i_1,\ldots,i_4\rangle,$$
$$|D'j\rangle = \sum_{i_1,\ldots,i_4} c'_{i_1,\ldots,i_4}\mathcal{S}|i_1,\ldots,i_4\rangle, \quad (4)$$

where c and c' with $c' = -c$ are exchange-dependent coefficients and $j = 1, 2$ and 3. For state $|D1\rangle$ ($|D'1\rangle$), we have $\langle S_1^z\rangle, \langle T_2^z\rangle > 0\,(< 0)$, and $\langle S_3^z\rangle, \langle T_4^z\rangle < 0\,(> 0)$, which result in a nonzero staggered magnetization in both the subsystems with spins S and T. In this phase, the ground state possesses uudd or dduu orders where u and d stand for up and down, respectively. Moreover, for state $|D2\rangle$ ($|D'2\rangle$), we have $\langle S_1^z\rangle, \langle T_2^z\rangle, \langle T_4^z\rangle > 0\,(< 0)$ and $\langle S_3^z\rangle < 0\,(> 0)$, which indicate that the ground state has uudu or ddud orders with a nonzero staggered magnetization in the subsystem with spin S and magnetization in the subsystem with spin T. Finally, in state $|D3\rangle$ ($|D'3\rangle$), $\langle S_1^z\rangle, \langle T_2^z\rangle, \langle S_3^z\rangle > 0\,(< 0)$ while $\langle T_4^z\rangle < 0\,(> 0)$, indicating uuud or dddu orders with a nonzero magnetization in the subsystem with spin S and nonzero staggered magnetization in the subsystem with spin T.

It is clearly seen that by increasing the three-site interaction, the magnetic orders (the green and blue colors) disappear and instead an AFQ order emerges. Actually, by increasing J_3, more product states contribute in the ground state which results in the disappearance of the magnetic orders. In the case of negative J_3, the ground state of the finite chain is magnetically disordered, except for some narrow intervals that the ground state is degenerate with magnetic order. In the following sections, we will show that all the mentioned orders also exist in the ground-state phase diagram of the infinite chain.

In the above discussions, we have made an important physical assumption on the ground state of the finite system, which we explain it as the following. In one-dimensional gapped spin chains with short-range interaction, the true ground state should follow the area law [59,60]. According to the area law, when the correlation between particles in a system reduces exponentially with distance, the entanglement

TABLE I. The definitions of various magnetic and nonmagnetic orders. m_S^z (m_T^z) and sm_S^z (sm_T^z) are, respectively, the magnetization and the staggered magnetization in the subsystem with spin S (T). Also, sm^z is the staggered magnetization of the entire system and **sq** shows the staggered quadrupole order in the subsystem with spin T.

Phase	Configuration	Order parameters
F	uuuu	m_S^z, m_T^z
N	dudu	m_S^z, m_T^z, sm^z
D1	uudd, duud	sm_S^z, sm_T^z
D2	uudu, duuu	sm_S^z, m_T^z
D3	dudd, uuud	m_S^z, sm_T^z
AFQ		**sq**

between one region and the rest of the system only depends on the area of the boundary between them. As a result, when the system is divided into two parts, only short-range correlations around the cut play a role in the ground-state entanglement. This is contrary to the excited states in which the entanglement follows a volume law. For a finite spin chain with a degenerate ground state, in the absence of an external magnetic field, the ground state is a linear combination of symmetry-broken degenerate states. In this state, the symmetry of the system is preserved and expectation values of all local order parameters are zero. Although such a state is the true ground state of the system, the entanglement in this state is high and consequently cannot help us reach the ground state of the infinite system. Therefore, to have a better intuition about the ground-state properties of our infinite spin chain from the ground state properties of a finite chain, it is more reasonable to choose a symmetry-broken quasiground state with lower entanglement.

III. CLASSICAL PHASE DIAGRAM

To obtain the classical phase diagram of our spin model, spins T and S are considered three-dimensional classical vectors, respectively, with sizes 1 and 1/2. By minimizing the classical energy of a finite spin chain described by the Hamiltonian Eq. (1) with respect to the polar and azimuthal angles of spins, we find that the configuration with minimum energy is coplanar and follows a four-sublattice structure. Therefore, to obtain the classical phase diagram, we parametrize the spin vectors as follows:

$$\begin{aligned}\vec{S}_i &= S(\cos\theta_i\hat{z} + \sin\theta_i\hat{x}),\\ \vec{T}_j &= T(\cos\theta_j\hat{z} + \sin\theta_j\hat{x}).\end{aligned} \tag{5}$$

By considering a four-sublattice structure, we have

$$\begin{aligned}\theta_{4i} &= \theta_{4i+4} = \theta_0,\\ \theta_{4i+1} &= \theta_{4i+5} = \theta_1,\\ \theta_{4i+2} &= \theta_{4i+6} = \theta_2,\\ \theta_{4i+3} &= \theta_{4i+7} = \theta_3.\end{aligned} \tag{6}$$

According to Eq. (6), obtaining the classical ground state is reduced to minimizing the classical energy of a four-site block $(S_0 - T_1 - S_2 - T_3)$,

$$\begin{aligned}E_{cl}/N = &\frac{J_1 ST}{2}(\cos\theta_0 + \cos\theta_2 + \cos\theta_{23} + \cos\theta_{30})\\ &+ J_2(S^2\cos\theta_{20} + T^2\cos\theta_3)\\ &+ J_3 S^2 T^2(\cos\theta_0\cos\theta_2 + \cos\theta_{23}\cos\theta_{30}),\end{aligned} \tag{7}$$

where $\theta_{ij} = \theta_i - \theta_j$, and $\theta_1 = 0$ (we choose the z axis along the T_1 direction). To present the classical phase diagram, we investigate the behavior of the staggered magnetization in different subsystems, defined as

$$\begin{aligned}sm^z &= \sum_i (-1)^{i+1} m_i^z / |m_i^z|,\\ sm_S^z &= \sum_i (-1)^{i+1} m_{2i}^z / |m_{2i}^z|,\\ sm_T^z &= \sum_i (-1)^{i+1} m_{2i+1}^z / |m_{2i+1}^z|.\end{aligned} \tag{8}$$

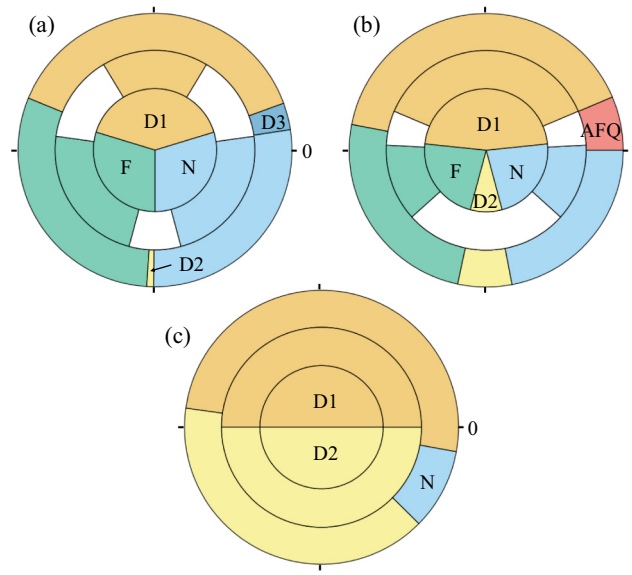

FIG. 2. The ground-state phase diagram of the frustrated mixed-spin (1,1/2) chains in the $J_1 - J_2$ plane for different values of $J_3 > 0$ [(a) $J_3 = 0.25$, (b) $J_3 = 0.75$, and (c) $J_3 = 1.5$]. The tick marks, respectively, show the angles $\phi = 0, \pi/2, \pi, 3\pi/2$ when we move counterclockwise on the circle. The inner, middle, and outer circles are, respectively, the results of classical approach, linear SWT, and CMFT. N and F refer to the phases with Neel and ferromagnetic orders, and D1, D2, and D3 are phases where the ground states are highly degenerate. In the AFQ, all the magnetic order parameters are zero, while staggered quadrupole order parameter is nonzero. All these orders are defined in Table I.

The classical phase diagrams of the Hamiltonian Eq. (1) are illustrated in Figs. 2 and 3 (the inner circles) for different positive and negative values of the three-site interaction. Two phases with F and N orders, and also different highly degenerate phases (D1, D2, and D3) are appeared in the classical phase diagrams. Since our spin system consists of two types of spin with different sizes, then, in general, we can classify all classical phases using the total magnetization of the ground state. Accordingly, except for the D1 phase, the other phases have a ferrimagnetic order with net total magnetization. But to examine the effects of quantum fluctuations in more detail, it is more reasonable to classify the phases by defining the subsystems' magnetization and staggered magnetization, as we have defined in Table I.

For small values of J_2, around $\phi = 0\,(\pi)$, for $J_3 < 1$, the system is in the N (F) phase, while for $J_3 > 1$, the strong three-site interactions destroy these orders, and instead the highly degenerate D1 and D2 phases appear. In the D1 phase, which appears for $J_2 > 0$, the spins in each subsystem are antiparallel to minimize both the NNN and three-site interactions, and both the uudd and duud configurations are the ground states. But in D2, which appears for $J_2 < 0$, these interactions are partially minimized by antiparallel alignment of $S = 1/2$ spins, while parallel alignment of $T = 1$ spins and the uudu and duuu configurations have minimum energy.

For large values of J_2, around $\phi = \pi/2$, the system is in the D1 phase for all positive and small negative strengths of J_3, while for large positive three-site interactions another

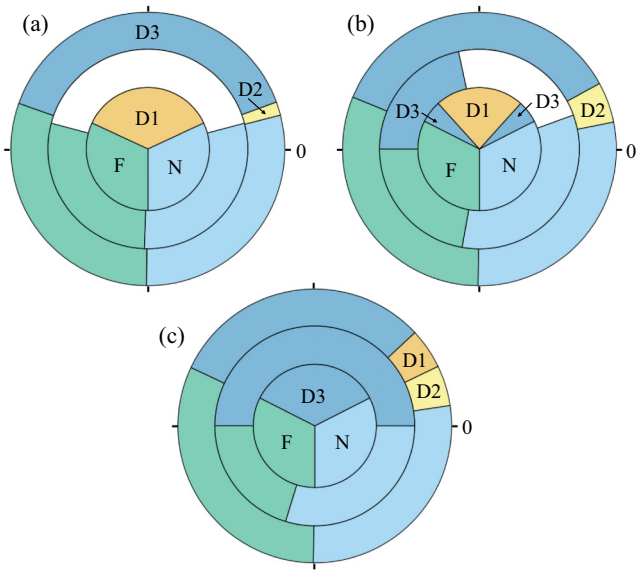

FIG. 3. The ground-state phase diagram of the frustrated mixed-spin (1,1/2) chains in the $J_1 - J_2$ plane for different values of $J_3 < 0$ [(a) $J_3 = -0.25$ (b) $J_3 = -0.75$, and (c) $J_3 = -1.5$]. See the caption of Fig. 2 for additional information.

degenerate phase, the D3 phase, appears in the ground-state phase diagram (see Fig. 2). In this phase, the dudd and uuud configurations have minimum energy.

For large strengths of $J_3 > 0$, for example, at $J_3 = 1.5$, the D1 phase is stabilized in the entire region of $J_2 > 0$ to minimize both the $J_2 > 0$ and J_3 interactions, while for $J_2 < 0$, the system is in the D2 phase to partially minimize both the $J_2 < 0$ and $J_3 > 0$ interactions [see Fig. 2(c)]. In the limit of strong $J_3 < 0$ interaction, for example, at $J_3 = -1.5$, all three N, F, and D3 phases minimize the three-site interactions, individually. For strong antiferromagnetic J_2 interaction, the D3 phase is stabilized to satisfy the J_2 interaction in subsystem T, while for small strengths of J_2 in both cases of $J_2 < 0$ and $J_2 > 0$, the ferromagnetic (N) phase is stabilized in favor of F (antiferromagnetic) NN interactions J_1 [see Fig. 3(c)].

It should be noted that in the D1, D2, and D3 phases, each block has two minimum energy configurations. This double degeneracy induces a large classical degeneracy of the order of $2^{N/2}$ in the system, which are often lifted by including quantum fluctuations. In the next sections, we employ different methods and investigate the stability of the classical phases against quantum fluctuations.

IV. SPIN-WAVE THEORY (SWT): SOFT MODES AND FLAT-BAND MAGNONS

As shown, in the classical phase diagrams there are three different highly degenerate phases. Considering quantum fluctuations by means of SWT can partially lift these degeneracies. In this section, we use linear SWT and obtain the ground-state phase diagram of our frustrated system, as well as excitation spectra.

As the spins lie on the xz plane, before performing SWT, we apply the following rotations:

$$\begin{pmatrix} S_i^x \\ S_i^y \\ S_i^z \end{pmatrix} = \mathcal{R}_y(\theta_i) \begin{pmatrix} \tilde{S}_i^x \\ \tilde{S}_i^y \\ \tilde{S}_i^z \end{pmatrix},$$
$$\begin{pmatrix} T_j^x \\ T_j^y \\ T_j^z \end{pmatrix} = \mathcal{R}_y(\theta_j) \begin{pmatrix} \tilde{T}_j^x \\ \tilde{T}_j^y \\ \tilde{T}_j^z \end{pmatrix}, \tag{9}$$

where θ_i and θ_j are obtained from Eqs. (5) and $\mathcal{R}_y(\theta)$ is a rotation matrix around the y axis, perpendicular to the spin plane. Using Holstein-Primakoff (HP) transformations, we turn the spin Hamiltonian Eq. (1) into a bosonic one. Unlike the F and N phases, in the degenerate phases the classical ground states are highly degenerate and it is not possible to use SWT for all configurations. We use the classical states of the forms: ... uudd ..., ... uudu ..., and ... uuud ..., respectively, for the D1, D2, and D3 phases. To get acceptable results, we must consider a ground state close to the exact ground state of the system. Since, except in few cases such as the F phase, the exact ground state of quantum spin models is not available, a classical ground state is used. The more similar this classical state is to the ground state of the system, the more precise the results of SWT will be. For example, in a spin chain with antiferromagnetic NN coupling, the classical ground state that is usually considered is a N state. Since this state is far from the quantum ground state, the results of the SWT are not valid. This is because the quantum fluctuations do not allow the N order to emerge in the ground state of the system. But if we consider the same classical state for an antiferromagnetic square lattice, the results of the SWT are acceptable and valid. In our case, since the selected states are stable in the presence of quantum fluctuations (according to our CVM results, see Sec. VI), therefore we expect the results of SWT to be valid.

In all these phases, the bosonic Hamiltonian has the following form:

$$H = E_{\rm cl} + \sum_k F(k) + \sum_k \psi_k^\dagger \mathbb{D}(k) \psi_k, \tag{10}$$

where $E_{\rm cl}$ is the classical energy, $F(k)$ is a function of bosons wave number, $\mathbb{D}(k)$ is a dynamical square matrix made up of the coefficients of bilinear terms, and ψ_k is a vector of HP bosonic creation and annihilation operators (see Appendix A). In the F, N, D2, and D3 phases, the dynamical matrix is positive-definite with nonzero positive eigenvalues, but, in contrast, in the D1 phase this matrix is semi-positive-definite with at least one zero eigenvalue. The dimension of the dynamical matrix is determined by the number of sublattices in each subsystems. In the F and N phases, the classical state has a two-sublattice structure, and therefore $\mathbb{D}$ is a 4×4 matrix. In the D2 (D3) phase, however, due to the translational symmetry breaking, in the $S = 1/2$ ($T = 1$) subsystem, we define three kinds of HP bosons to fully capture the excitations and corrections to the classical phase diagram, and therefore the $\mathbb{D}$ matrix in these phases is a 6×6 matrix with three positive eigenvalues.

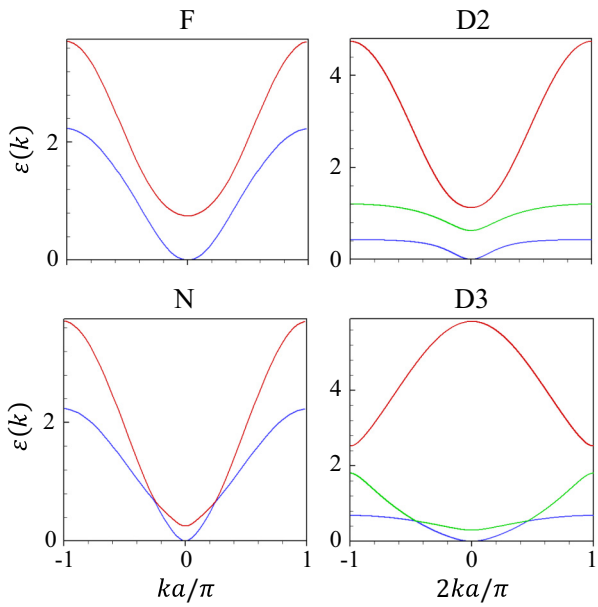

FIG. 4. Magnon dispersion in different phases of the $J_1 - J_2 - J_3$ mixed-spin (1,1/2) chains. For the F phase, we set $J_3 = 0.25$ and $\phi = 240°$; for N, $J_3 = 0.25$ and $\phi = 300°$; for D2, $J_3 = 1.5$ and $\phi = 300°$; and for D3, $J_3 = -1.5$ and $\phi = 110°$. The mentioned angles, respectively, correspond to the following (J_1, J_2) pairs: F, $(-0.5, -0.87)$; N, $(0.5, -0.87)$; D2, $(0.5, -0.87)$; and D3, $(-0.34, 0.94)$.

A. The D2 and D3 phases with dispersive magnons

Paraunitary diagonalization [61–63] of the dynamical matrix $\mathbb{D}$, yields the ground state of the Hamiltonian Eq. (10) as well as the magnon excitations. In Fig. 4, we have plotted the excitation energies in the different F, N, D2, and D3 phases. In all phases, the lowest-energy excitation is gapless and behaves as k^2 near $k = 0$ point. In the absence of J_2 and J_3 interactions, linear SWT yields two types of magnons: a gapless acoustical branch with $S^z = N/2 - 1$ and a gapped optical branch with $S^z = N/2 + 1$, respectively, with the dispersions ε_k^- and ε_k^+, given by $\varepsilon_k^{\mp}/J_1 = \mp\frac{1}{2} + (\frac{1}{4} + 2\sin^2 k)^{1/2}$, though the antiferromagnetic gap within the linear SWT is $\Delta = J_1$. Adding NNN and three-site interactions leads to changes in the spectrum. In the F phase, the antiferromagnetic gap increases, while decreasing in the N phase. In contrast to the standard case where the two branches have finite separation in the entire Brillouin zone, here in the N phase, some band-crossing occurs at a finite k value.

In the D2 phase, the bottom and top of all magnon bands are, respectively, located at $k = 0$ (the zone origin) and $k = \pi/(2a)$ (taking into account that $2a$ corresponds to the size of the unit cell for D phases—this point is the zone boundary), and no band crossing happens. The lowest-energy excitation is gapless, while the other two branches are separated by an energy gap from the ground state, larger than the gap in the standard case. In the D3 phase, unlike D2, the bottom of the highest-energy magnon band is located at the zone boundary, meaning that the configuration where each magnon is out of phase with its neighbors has the lowest energy. Furthermore, for stronger J_3 interactions, we see that the highest-energy bands in both the D2 and D3 phases [red curves in Fig. 4 (D2 and D3)] become more disperse in energy, and successively weaker J_3 interactions correspond to flatter bands [blue and red curves in Fig. 4 (F and N)].

B. The D1 phase and flat-band magnons

In the D1 phase, we use the classical ground state of the form $\ldots$uudd$\ldots$. Due to the translational symmetry breaking in both the subsystems, we consider four HP bosons in our SWT. The spin-wave Hamiltonian is given by Eq. (10), with ψ_k being a vector given by $\psi_k = (a_k, b_k, c_k, d_k, a_k^\dagger, b_k^\dagger, c_k^\dagger, d_k^\dagger)^\dagger$, where the eight components are HP bosonic annihilation/creation operators, and the dynamical matrix is given by

$$\mathbb{D} = \begin{pmatrix} A & B \\ B* & A* \end{pmatrix},$$

with A and B being the following square matrices:

$$A = \begin{pmatrix} f^- & g^+ e^{-ik} & 0 & 0 \\ g^+ e^{ik} & \frac{1}{2}(J_2 + J_3) & 0 & 0 \\ 0 & 0 & f^+ & 0 \\ 0 & 0 & 0 & \frac{J_2}{2} \end{pmatrix},$$

$$B = \begin{pmatrix} 0 & 0 & -\frac{J_2}{4} e^{-2ik} & 0 \\ 0 & 0 & g^- e^{-ik} & -\frac{J_2}{2} e^{-2ik} \\ -\frac{J_2}{4} e^{-2ik} & g^- e^{-ik} & 0 & 0 \\ 0 & -\frac{J_2}{2} e^{-2ik} & 0 & 0 \end{pmatrix},$$

where the parameters $f^\pm$ and $g^\pm$ are defined in Eq. (A2). The function $F(k)$ in the Hamiltonian Eq. (10) is obtained as $F(k) = -\mathrm{Tr}(A)$, where Tr denotes the trace. Unlike the F, N, D2, and D3 phases, in the D1 phase the dynamical matrix is semi-positive-definite. Using an appropriate paraunitary transformation [61–63], the spin-wave Hamiltonian Eq. (10) is diagonalized as

$$\begin{aligned} H &= E_{sw} + H_s + H_{ns}, \\ H_s &= \varepsilon_1 \sum_k \alpha_k^\dagger \alpha_k + \varepsilon_2 \sum_k \beta_k^\dagger \beta_k, \\ H_{ns} &= \sum_k (\gamma_k^\dagger \gamma_k + \gamma_k \gamma_k^\dagger + \gamma_k \gamma_k + \gamma_k^\dagger \gamma_k^\dagger) \\ &\quad + \sum_k (\eta_k^\dagger \eta_k + \eta_k \eta_k^\dagger - \eta_k \eta_k - \eta_k^\dagger \eta_k^\dagger), \end{aligned} \tag{11}$$

where, α_k, β_k, γ_k, and η_k ($\alpha_k^\dagger$, $\beta_k^\dagger$, $\gamma_k^\dagger$, and $\eta_k^\dagger$) are magnonic creation (annihilation) operators, and E_{sw} is the ground-state energy which is the classical energy modified by quantum corrections. The Hamiltonian H_s, has the standard form of a diagonalized bosonic Hamiltonian, where ε_1 and ε_2 are some positive constants independent of the k values of the magnons α and β. The Hamiltonian H_{ns} is, however, not in the standard form, and to obtain the energy spectrum of the γ and η magnons, we use the inverse Dirac transformations, write the bosonic operators in terms of the position and momentum

operators, and readily obtain

$$\gamma_k^\dagger\gamma_k + \gamma_k\gamma_k^\dagger + \gamma_k\gamma_k + \gamma_k^\dagger\gamma_k^\dagger = X_k^2,$$
$$\eta_k^\dagger\eta_k + \eta_k\eta_k^\dagger - \eta_k\eta_k - \eta_k^\dagger\eta_k^\dagger = P_k^2. \quad (12)$$

As seen, the bosonic Hamiltonian is written in terms of the position and momentum operators which are independent and have continuous spectrum, running from 0 to infinity. The spectrum is twofold degenerate: the eigenvalues x and $-x$ of the operator X correspond to different wave functions (Dirac delta functions). These modes, i.e., γ and η are improper soft modes corresponding to zero eigenvalue and zero paravalues of the dynamical matrix D in (IV B). To sum up, in the D1 phase all magnons are amazingly dispersionless, which is a crucial feature for magnon localization and magnon crystallization. The crystallization of magnetic quasiparticles, like a Wigner crystal, could be key to understanding exotic quantum phases such as supersolid phases [64,65] and flat-band solid states [66]. Localization of magnons occurs in various one- and two-dimensional systems [67] (see also the review paper [68] by Derzhko *et al.* and references therein). The mechanism behind such a crystallization is different in different systems. In many cases, this localization, in turn, is a consequence of destructive quantum interference which occurs due to a special geometry of the lattice. In frustrated spin dimer systems in the presence of an applied magnetic field, when repulsive interactions of magnons become large, they completely suppress the hopping of magnons and, consequently, a periodic array of magnons form [69]. Although the mechanisms are different, in all systems frustration plays a vital role in the formation of the dimer phase and, consequently, the crystallization of magnons. In our mixed-spin system, the presence of NNN and three-site interactions causes the system to be frustrated. If the NNN interactions are weaker than the NN ones, magnon crystal forms only in the presence of three-site interaction. It seems that the quadrupoles in the system cause the quantum interference of the magnons to be destructive—they cause the magnons to be flat-band and localized in each unit cell.

Finally, in Figs. 2 and 3, we have plotted the spin wave ground-state phase diagrams (the middle circles) of the Hamiltonian Eq. (1). In general, the quantum fluctuations given by linear SWT modify the classical orders around transition points and shift phases boundaries. However, in the regions illustrated by white colors, the SWT fails to predict the order of the system, properly. It predicts that the fluctuations destabilize the degenerate phases. It takes into account the effects of quantum fluctuations but does not give more information about the degenerate phases in comparison with the classical method, and we should employ other techniques to obtain the ground-state phase diagram.

V. CLUSTER MEAN FIELD THEORY: ANTIFERROQUADRUPOLAR ORDER

CMFT is an extension of the standard mean-field theory in which the interacting spin system is reduced to a noninteracting system of clusters of multiple sites. In this theory, the interactions of spins within the clusters are treated, exactly, and the outside spins are included as effective fields. In this approach, quantum fluctuations as well as spin correlations are partially taken into account [64,65,70–73]. In this section, we use CMFT and obtain the ground-state phase diagram of our frustrated mixed-spin system for different strengths of the NN, NNN, and three-site interactions. We will show that, aside from the F and N phases, our CMFT predicts the emergence of a nonmagnetic AFQ order.

By dividing the system into clusters of four spins (two $S = 1/2$, and two $T = 1$ spins), we write the Hamiltonian Eq. (1) as

$$\begin{aligned} H_{\mathrm{CMFT}} &= \sum_{i=0}^{N/2}\left(H_i + h_i^{\mathrm{eff}}\right), \\ H_i &= J_1(\vec{S}_{2i}\cdot\vec{T}_{2i+1} + \vec{T}_{2i+1}\cdot\vec{S}_{2i+2} + \vec{S}_{2i+2}\cdot\vec{T}_{2i+3}) \\ &\quad + J_2(\vec{S}_{2i}\cdot\vec{S}_{2i+2} + \vec{T}_{2i+1}\cdot\vec{T}_{2i+3}) \\ &\quad + J_3(\vec{S}_{2i}\cdot\mathbf{Q}_{2i+1}\cdot\vec{S}_{2i+2}), \\ h_i^{\mathrm{eff}} &= J_1(\vec{m}_{2i-1}\cdot\vec{S}_{2i} + \vec{T}_{2i+3}\cdot\vec{m}_{2i+4}) \\ &\quad + J_2(\vec{m}_{2i-2}\cdot\vec{S}_{2i} + \vec{S}_{2i+2}\cdot\vec{m}_{2i+4} + \vec{m}_{2i-1}\cdot\vec{T}_{2i+1} \\ &\quad + \vec{T}_{2i+3}\cdot\vec{m}_{2i+5}) + J_3(\vec{m}_{2i-2}\cdot\mathbf{q}_{2i-1}\cdot\vec{S}_{2i} \\ &\quad + \vec{S}_{2i+2}\cdot\mathbf{Q}_{2i+3}\cdot\vec{m}_{2i+4}), \end{aligned} \quad (13)$$

where $\mathbf{Q}_i$ is quadrupole operator with the components $(T_i^x)^2 - (T_i^y)^2$, $\frac{1}{\sqrt{3}}[2(T_i^z)^2 - (T_i^x)^2 - (T_i^y)^2]$, $T_i^xT_i^y + T_i^yT_i^x$, $T_i^yT_i^z + T_i^zT_i^y$, and $T_i^xT_i^z + T_i^zT_i^x$ [74–76], and $\mathbf{q}_i$ is quadrupole tensor with quadrupole moment $\mathbf{q}_i = \langle\mathbf{Q}_i\rangle$, where the bracket $\langle\rangle$ denotes expectation values on the CMF ground state. In CMFT, the three-site four-spin interaction term is transformed to the interaction of two dipoles with a quadrupole and to obtain the CMF ground- phase diagram, we define the following staggered quadrupole order parameters:

$$\mathbf{sq} = \sum_i (-1)^{i+1}\mathbf{q}_{2i+1}/|\mathbf{q}_{2i+1}|, \quad (14)$$

where the summation runs over spins T. The CMF phase diagrams are demonstrated in Figs. 2 and 3 (the outer circles) for different strengths of $J_3 > 0$ and $J_3 < 0$. The quantum fluctuations considered in CMFT cause changes in the classical phase diagram, which can be referred to the appearance of the AFQ order in the case of $J_3 > 0$ [see Fig. 2(b) for $J_3 = 0.75$]. In this phase, the staggered quadrupole order in the subsystem with the T spins is nonzero, but all magnetic orders are zero.

Despite all abilities of the CMFT in improving the classical phase diagram of the system, it fails to predict the feature of the degenerate phases. Nevertheless, one can use CMFT and implement a CVM to find the features of the degenerate phases. In the following, we employ a CMFT-based CVM and obtain the ground-state phases in the degenerate regions.

VI. CLUSTER VARIATIONAL METHOD (CVM)

In CVM, a many-body wave function is estimated by a family of variational wave functions of finite blocks which make up that system [77]. In this respect, some properties of the many-body wave function, like long-range entanglement, which were not considered in CMFT, return to the system. This method is useful in cases that the optimum configuration obtained in the blocks is highly degenerate. Here, we

generalized the CVM presented in Ref. [77] to our mixed-spin Hamiltonian Eq. (1) and obtain the ground states in the degenerate regions of the CMFT phase diagram.

In CVM, the variational wave function of the system ($|\varphi^{\rm CVM}\rangle$) is written as a superposition of the highly degenerate wave functions,

$$|\varphi^{\rm CVM}\rangle = \sum_{\{\vec{m}\}} a_{\{\vec{m}\}} |\psi(\{\vec{m}\})\rangle, \tag{15}$$

where the sum runs over all $2^{N/2}$ configurations which optimize the variational energy of the system, and $|\psi(\{\vec{m}\})\rangle$ is the wave function of the system with configuration $\{\vec{m}\}$ [see Eq. (B1)]. The complex coefficients $a_{\{\vec{m}\}}$ are variational parameters, satisfying

$$\sum_{\{\vec{m}\}} |a_{\{\vec{m}\}}|^2 = 1. \tag{16}$$

The variational energy is given by

$$E_{\rm CVM} = \frac{\langle\varphi^{\rm CVM}|H|\varphi^{\rm CVM}\rangle}{\langle\varphi^{\rm CVM}|\varphi^{\rm CVM}\rangle} = \frac{\sum_{\{\vec{m}'\}\{\vec{m}\}} a^*_{\{\vec{m}'\}} a_{\{\vec{m}\}} X_{\{\vec{m}'\}\{\vec{m}\}}}{\sum_{\{\vec{m}'\}\{\vec{m}\}} a^*_{\{\vec{m}'\}} a_{\{\vec{m}\}} O_{\{\vec{m}'\}\{\vec{m}\}}} = \frac{\mathbf{a}^\dagger \cdot \mathbf{X} \cdot \mathbf{a}}{\mathbf{a}^\dagger \cdot \mathbf{O} \cdot \mathbf{a}}, \tag{17}$$

where $\mathbf{a}$ is a vector of the variational coefficients and $\mathbf{O}$ and $\mathbf{X}$ are matrices with the following elements:

$$O_{\{\vec{m}'\}\{\vec{m}\}} = \langle\psi(\{\vec{m}'\})|\psi(\{\vec{m}\})\rangle,$$
$$X_{\{\vec{m}'\}\{\vec{m}\}} = \langle\psi(\{\vec{m}'\})|H|\psi(\{\vec{m}\})\rangle, \tag{18}$$

which are the overlap of the degenerate wave functions and the matrix elements of the Hamiltonian in this basis, respectively [77]. Minimizing the variational energy with respect to the coefficients gives the ground state. The details of our CVM are reported in Appendix B. Since in the CVM the interactions between nearest-neighbor clusters are taken into account properly, we expect to see features of highly entangled phases such as quantum SL in our mixed-spin model. Actually, such phases cannot be predicted by CMFT, because in CMFT the interactions between clusters are considered as mean fields.

In Figs. 5 and 6, we have plotted the final ground-state phase diagrams of the Hamiltonian Eq. (1) for different strengths of the three-site interaction. Using the CVM, the degeneracies of the ground states in D1, D2, and D3 phases are lifted and instead the nondegenerate uudd, duuu, and dudd phases, and also the nonmagnetic AFQ order emerges in the ground-state phase diagram. But the interesting point is the emergence of a disordered phase for large strengths of three-site interactions, where all the magnetic and the quadrupole order parameters are zero, and the ground state has no long-range order. Such a disordered phase is also seen by our CVM in the ground-state phase diagram of the $J_1 - J_3$ mixed-spin models ($J_2 = 0$). Recently, using the density matrix renormalization group (DMRG) method, it has been shown that in the $J_1 - J_3$ model this phase is a kind of SL phase [55]. This means that our CVM can properly predict the presence of such a SL phase in the ground-state phase diagram of frustrated mixed-spin systems. However, to conclude that the SL region in our system is definitely a SL phase, the behavior of correlation functions should be examined. Although

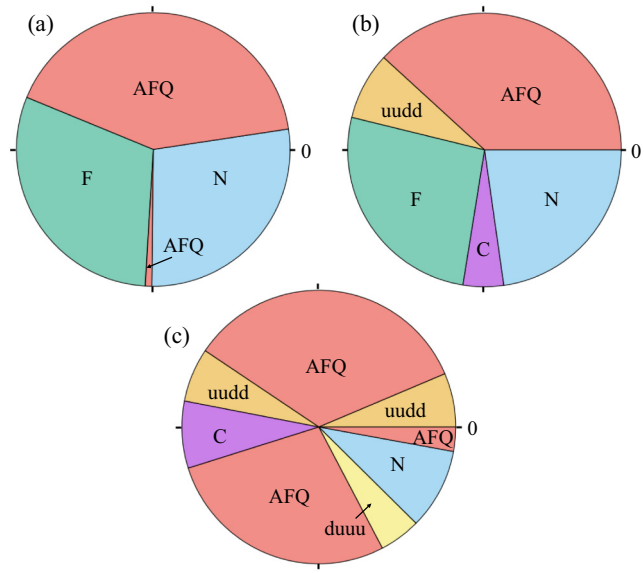

FIG. 5. The ground state phase diagram of the frustrated mixed-spin (1,1/2) chains in the $J_1 - J_2$ plane, for different values of $J_3 > 0$ [(a) $J_3 = 0.25$ (b) $J_3 = 0.75$ and (c) $J_3 = 1.5$]. The tuning parameter is the angle ϕ. The uudd phase in which the magnons are flat-band, is not seen for small strengths of three-site interactions.

we cannot calculate the correlation functions by CVM, but since the CVM wave function is a linear combination of the degenerate states, and also all the local order parameters are zero, the SL region is most likely to be a true SL phase.

There is also a region denoted by C in which with the precision we considered in our CVM, the true order of the

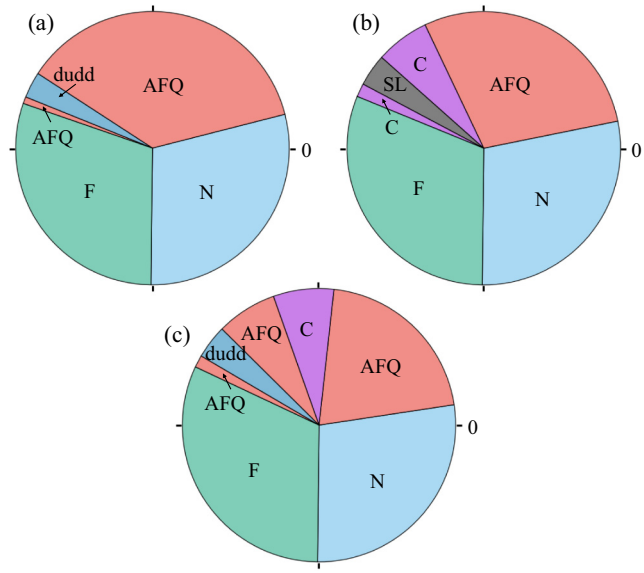

FIG. 6. The ground state phase diagram of the frustrated mixed-spin (1,1/2) chains in the $J_1 - J_2$ plane, for different values of $J_3 < 0$ ((a) $J_3 = -0.25$, (b) $J_3 = -0.75$ and (c) $J_3 = -1.5$). The tuning parameter is the angle ϕ. The SL phase emerges for large strengths of three-site interactions. This phase is absent in the phase diagrams illustrated in Fig. 5.

ground state is not fixed. In this region, by varying J_1 and J_2 the ground state oscillates sequentially between magnetic and AFQ orders.

To have a better understanding of our final ground-state phase diagram, reported in Figs. 5 and 6, in the following we discuss our results in the two extreme limits of (1) $J_1, J_3 \neq 0$, and $J_2 = 0$, and (2) $J_2, J_3 \neq 0$, and $J_1 = 0$. In the absence of J_2, when $J_3 = 0$ we have a ferrimagnetic spin-(1,1/2) chain with ferrimagnetic order indicating by both the $sm^z \neq 0$ and $m^z \neq 0$. When J_3 becomes nonzero, we are faced with two different situations for negative and positive values of J_3. For the former case ($J_3 < 0$), the ferrimagnetic order of the chains will remain unchanged, for $J_1 > 0$ the alignment of spins is antiparallel and the ground state has a N order, and for $J_1 < 0$ the alignment is parallel and the ground state has a F order. But, in case of positive J_3, in the limit of large J_3 the ferrimagnetic order of the system is destroyed and instead the AFQ (C) phase appears for $J_1 > 0$ ($J_1 < 0$).

Now let us go to the limit of $J_2, J_3 \neq 0$, and $J_1 = 0$. In the absence of J_1, when $J_3 = 0$, we have two decoupled spin chains, one is a spin-1/2 and the other is a spin-1 chain. When $J_2 < 0$, trivially both spin chains have a F ground state with magnon excitations, but for $J_2 > 0$, we have a critical spin-1/2 chain with a gapless ground state and spinon excitations, and a spin-1 chain with a gapped ground state and Haldane excitations. The addition of the three-site interactions has interesting effects. When $J_3 < 0$, in the case of $J_2 < 0$, the F orders of the chains remain unchanged and a ferrimagnetic order with two kinds of magnon excitations is formed in the mixed-spin chain. But, in the case of $J_2 > 0$, an AFQ order appear in the mixed-spin chain to minimize both the J_2 and J_3 interactions. When $J_3 > 0$, the three-site interactions destroy the F orders of the spin-1/2 and spin-1 chains and instead the AFQ or C phases appear for the entire range of $J_2 < 0$, and large J_3. The interesting point to note is that even though in the case of positive J_2 both the spin-1/2 and the spin-1 chains are disordered, but the presence of three-site interaction causes the appearance of the AFQ order in the mixed-spin chain.

To find the SL regions in our model, we have also plotted in Fig. 7 the $J_2 - J_3$ phase diagram of our frustrated mixed-spin (1,1/2) system in the units of J_1. At the $J_3 = 0$ line, the ground-state phase diagram of the system is well-known [54]. Using DMRG, it has been shown that below the $J_2 = 0.231$ point, the ground state is in the ferrimagnetic N phase with total spin $S_g = (T - S)N$, and above this point the ground state is disordered with $S_g = 0$. In agreement with the DMRG, our CVM also predicts a magnetically ordered-disordered phase transition around $J_2 \sim 0.3$. According to our CVM results, in the absence of three-site interaction, for low strengths of J_2 the ground state has N order, by increasing J_2 the effects of frustration become much bolder and above the transition point, in the region of $0.3 < J_2 < 1.2$, the convergence to a ground state does rarely happen (in this interval, our CVM often predicts a uudd phase), but above this region the AFQ order appears in the ground state. By introducing J_3, in addition to the AFQ phase, other nonmagnetic phases such as the uudd and SL also appear in the phase diagram.

Furthermore, as clearly seen from the phase diagrams in Figs. 5–7, the uudd phase is stable against quantum fluctuations. As we have discussed, in this phase magnon excitations

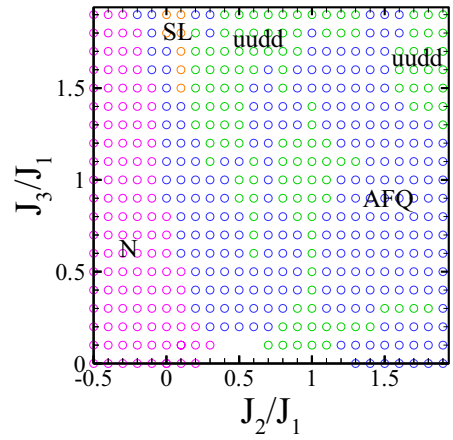

FIG. 7. The ground-state phase diagram of the frustrated mixed-spin (1,1/2) system for $J_1 = 1$ in the $J_2 - J_3$ plane. In the narrow regions for small positive J_2/J_1 and large positive J_3/J_1, the system is in the SL phase. In the wide green region, the system is in the uudd phase where magnons are flat band.

are flat band, and therefore magnon crystal can form in the system. The higher the strength of the three-site interactions, the greater the regions associated with the magnon crystal. This means that in the $J_1 - J_2 - J_3$ mixed-spin (1,1/2) chains, the presence of positive three-spin interactions is crucial in magnon crystallization.

VII. SUMMARY AND CONCLUSION

We investigated the ground-state phase diagram of frustrated mixed-spin (1, 1/2) chains with NN, NNN, and three-site four spins interactions. We first studied the classical phase diagrams and showed that, aside from the F and N orders, various kinds of highly degenerate phases emerge in the classical phase diagram. To consider the effects of quantum fluctuations, we studied the ground-state phase diagram of the system using SWT, CMFT, and CVM. We demonstrated that the degeneracies in the classical phase diagrams are lifted, and instead different exotic quantum orders, such as AFQ phase and SL appear in the ground-state phase diagram of the system. We also demonstrated that the ground state shows the magnetic uudd phase in which magnon hoppings are suppressed. In this phase, the magnons are flat band and magnon crystal can be formed in the system. Such a crystallization is indeed a consequence of the frustration and inhomogeneity of our mixed-spin system and is not seen in the frustrated $J_1 - J_2 - J_3$ spin-1 chains. As far as we know, except for the three dimensional flat-band metallic ferrimagnets, like $TbMn_6Sn_6$ [78], this is the first work in which flat-band magnons are seen in one-dimensional mixed-spin systems.

ACKNOWLEDGMENTS

The authors would like to thank O. Derzhko, H. R. Kazemi, and O. Benton for useful discussions. We also thank S. Alireza Ghasemi for discussions on our numerical simulations.

APPENDIX A: SPIN-WAVE HAMILTONIAN

In this Appendix, we obtain the spin-wave Hamiltonian of the $J_1 - J_2 - J_3$ mixed-spin (1,1/2) chains. In all the mentioned phases, the SW Hamiltonian is written as

$$H = E_{cl} + \sum_k F(k) + \sum_k \psi_k^\dagger \mathbb{D}(k)\psi_k, \tag{A1}$$

where E_{cl} is the classical ground-state energy. Making use of the following definitions:

$$\begin{aligned} a_1^\pm &= \frac{1}{2}(J_2(\cos(2k)-1) - 2J_3 \pm 2J_1), \\ a_2^\pm &= \frac{1}{2}(2J_2(\cos(2k)-1) - J_3 \pm J_1), \\ g^\pm &= \frac{\sqrt{2}}{4}(\pm J_1 - J_3), \quad f^\pm = \frac{1}{2}\left(J_3 + \frac{J_2}{2} \pm J_1\right), \\ h &= \frac{1}{2}(2J_2(\cos(2k)-1) + J_3),\ d = \frac{1}{2}(J_2 - J_1 - J_3), \end{aligned} \tag{A2}$$

the dynamical matrix $\mathbb{D}$, the vector ψ_k, and the function $F(k)$ are given as follows.

In the F and N phases, the vector ψ_k is $(a_k, b_k, a_{-k}^\dagger, b_{-k}^\dagger)$, where $a_k^\dagger(a_k)^\dagger$ and $b_k^\dagger(b_k)$ are the creation (annihilation) operators of HP bosons with wave number k. The dynamical matrix is the following 4×4 matrix:

$$\mathbb{D} = \begin{pmatrix} A & B \\ B & A \end{pmatrix},$$

where A and B are 2×2 square matrices, in the F phase they are

$$A = \begin{pmatrix} a_1^- & -2g^-\cos k \\ -2g^-\cos k & a_2^- \end{pmatrix},$$
$$B = \begin{pmatrix} 0 & 0 \\ 0 & 0 \end{pmatrix},$$

and in the N phase, we have

$$A = \begin{pmatrix} a_1^+ & 0 \\ 0 & a_2^+ \end{pmatrix},$$
$$B = \begin{pmatrix} 0 & -2g^+\cos k \\ -2g^+\cos k & 0 \end{pmatrix}.$$

The functions $F(k)$ are given by

$$F(k) = \tfrac{3}{2}J_2\cos(2k) - \mathrm{Tr}(A), \tag{A3}$$

where Tr denotes the trace.

In the D2 and D3 phases, the vector ψ_k is $(a_k, b_k, c_k, a_{-k}^\dagger, b_{-k}^\dagger, c_{-k}^\dagger)^\dagger$ and the dynamical matrix is 6×6 with A and B being 3×3 matrices; in the D2 phase, they are given by

$$A = \begin{pmatrix} f^- & g^+e^{ik} & 0 \\ g^+e^{-ik} & h & 0 \\ 0 & 0 & f^+ \end{pmatrix},$$
$$B = \begin{pmatrix} 0 & 0 & -\frac{J_2}{4}e^{2ik} \\ 0 & 0 & g^-e^{ik} \\ -\frac{J_2}{4}e^{-2ik} & g^-e^{-ik} & 0 \end{pmatrix},$$

and we have

$$F(k) = J_2\cos(2k) - \mathrm{Tr}(A), \tag{A4}$$

and in the D3 phase they are

$$A = \begin{pmatrix} a_1^- & -2g^-\cos k & 0 \\ -2g^-\cos k & d & 0 \\ 0 & 0 & \frac{J_2}{2} \end{pmatrix},$$
$$B = \begin{pmatrix} 0 & 0 & 0 \\ 0 & 0 & -\frac{J_2}{2}e^{ik} \\ 0 & -\frac{J_2}{2}e^{-ik} & 0 \end{pmatrix},$$

and $F(k) = \frac{J_2}{2}\cos(2k) - \mathrm{Tr}(A)$. All the dynamical matrices in the F, N, D2, and D3 phases are positive-definite. Using appropriate paraunitary transformations, we diagonalized these matrices and obtained the magnonic band structures of the system (see Fig. 4) as well as the ground-state phase diagram.

APPENDIX B: THE DETAIL CALCULATIONS OF THE CVM

To calculate the matrix elements $X_{\{\vec{m}'\}\{\vec{m}\}}$ and $O_{\{\vec{m}'\}\{\vec{m}\}}$, we need to know the single block wave functions $|\phi_i(\{\vec{m}\})\rangle$, which construct the degenerate wave function of the system as

$$|\psi(\{\vec{m}\})\rangle = \prod_i^{N/2} |\phi_i(\{\vec{m}\})\rangle, \tag{B1}$$

where the direct product runs over the blocks of the system. We rewrite the Hamiltonian Eq. (1) as a sum of two terms; H_i and $H'_{i,j}$, which include the intrablocks and the interblocks interactions, respectively. In our case, we divide the system into four-site blocks and write the Hamiltonian as

$$H_{\mathrm{CVM}} = \sum_i H_i + (H'_{i-1,i} + H'_{i,i+1})/2,$$

where

$$\begin{aligned} H_i = {} & J_1(\vec{S}_{2i}\cdot\vec{T}_{2i+1} + \vec{T}_{2i+1}\cdot\vec{S}_{2i+2} + \vec{S}_{2i+2}\cdot\vec{T}_{2i+3}) \\ & + J_2(\vec{S}_{2i}\cdot\vec{S}_{2i+2} + \vec{T}_{2i+1}\cdot\vec{T}_{2i+3}) \\ & + J_3(S_{2i}\cdot Q_{2i+1}\cdot S_{2i+2}), \end{aligned} \tag{B2}$$

and the interactions between nearest-neighbor blocks are given by

$$\begin{aligned} H'_{i-1,i} = {} & J_1(\vec{T}_{2i-1}\cdot\vec{S}_{2i}) + J_2(\vec{S}_{2i-2}\cdot\vec{S}_{2i} + \vec{T}_{2i-1}\cdot\vec{T}_{2i+1}) \\ & + J_3(S_{2i-2}\cdot Q_{2i-1}\cdot S_{2i}) \end{aligned}$$

and

$$\begin{aligned} H'_{i,i+1} = {} & J_1(\vec{T}_{2i+3}\cdot\vec{S}_{2i+4}) + J_2(\vec{S}_{2i+2}\cdot\vec{S}_{2i+4} + \vec{T}_{2i+3}\cdot\vec{T}_{2i+5}) \\ & + J_3(\vec{S}_{2i+2}\cdot Q_{2i+3}\cdot\vec{S}_{2i+4}). \end{aligned}$$

Therefore, the matrix elements of the Hamiltonian are written as

$$\begin{aligned} X_{\{\vec{m}'\}\{\vec{m}\}} &= \sum_i \langle\psi(\{\vec{m}'\})|H_i + (H'_{i-1,i} + H'_{i,i+1})/2|\psi(\{\vec{m}\})\rangle \\ &= \sum_i \{\langle\phi_i(\{\vec{m}'\})|H_i|\phi_i(\{\vec{m}\})\rangle \prod_{j\neq i} \langle\phi_j(\{\vec{m}'\})||\phi_j(\{\vec{m}\})\rangle \\ &\quad + \frac{1}{2}\langle\phi_i(\{\vec{m}'\})| \otimes \langle\phi_{i-1}(\{\vec{m}'\})|H'_{i-1,i}|\phi_{i-1}(\{\vec{m}\})\rangle \otimes |\phi_i(\{\vec{m}\})\rangle \prod_{k\neq i,i-1} \langle\phi_k(\{\vec{m}'\})||\phi_k(\{\vec{m}\})\rangle \\ &\quad + \frac{1}{2}\langle\phi_{i+1}(\{\vec{m}'\})| \otimes \langle\phi_i(\{\vec{m}'\})|H'_{i,i+1}|\phi_i(\{\vec{m}\})\rangle \otimes |\phi_{i+1}(\{\vec{m}\})\rangle \prod_{k\neq i,i+1} \langle\phi_k(\{\vec{m}'\})||\phi_k(\{\vec{m}\})\rangle\}. \end{aligned} \tag{B3}$$

Minimizing the variational energy, E_{CVM}, with respect to the variational parameters $a_{\{\vec{m}\}}$ results in the CVM wave function. To this end, we introduce a different normalized vector $\mathbf{b}$, as

$$\mathbf{a} = \mathbf{O}^{-1/2} \cdot \mathbf{b}$$

and write the CVM energy in Eq. (17) as

$$E_{\mathrm{CVM}} = \mathbf{b}^{\dagger} \cdot H'_{\mathrm{CVM}} \cdot \mathbf{b}, \tag{B4}$$

where

$$H'_{\mathrm{CVM}} = \mathbf{O}^{-1/2} \cdot H_{\mathrm{CVM}} \cdot \mathbf{O}^{-1/2}. \tag{B5}$$

Finally, the optimal superposition of the variational parameters $a_{\{\vec{m}\}}$ is given by the ground state of the Hamiltonian H'_{CVM}. These coefficients construct the CVM wave function in Eq. (15), which is useful for calculating order parameters.

[1] R. Coldea, S. M. Hayden, G. Aeppli, T. G. Perring, C. D. Frost, T. E. Mason, S.-W. Cheong, and Z. Fisk, Phys. Rev. Lett. **86**, 5377 (2001).

[2] F. Pratt, P. Baker, S. Blundell, T. Lancaster, S. Ohira-Kawamura, C. Baines, Y. Shimizu, K. Kanoda, I. Watanabe, and G. Saito, Nature (London) **471**, 612 (2011).

[3] U. Falk, A. Furrer, H. U. Güdel, and J. K. Kjems, Phys. Rev. Lett. **56**, 1956 (1986).

[4] A. Furrer and O. Waldmann, Rev. Mod. Phys. **85**, 367 (2013).

[5] U. Köbler, R. Mueller, L. Smardz, D. Maier, K. Fischer, B. Olefs, and W. Zinn, Z. Phys. B **100**, 497 (1996).

[6] N. Uryû and S. Friedberg, Phys. Rev. **140**, A1803 (1965).

[7] T. Iwashita and N. Uryû, J. Phys. Soc. Jpn. **36**, 48 (1974).

[8] Y. Yoshida, S. Schröder, P. Ferriani, D. Serrate, A. Kubetzka, K. von Bergmann, S. Heinze, and R. Wiesendanger, Phys. Rev. Lett. **108**, 087205 (2012).

[9] M. Roger, J. Hetherington, and J. Delrieu, Rev. Mod. Phys. **55**, 1 (1983).

[10] K. Kamase, K. Osaki, and N. Uryû, Phys. Lett. A **73**, 241 (1979).

[11] P. Ferriani, K. von Bergmann, E. Y. Vedmedenko, S. Heinze, M. Bode, M. Heide, G. Bihlmayer, S. Blügel, and R. Wiesendanger, Phys. Rev. Lett. **101**, 027201 (2008).

[12] P. Kurz, G. Bihlmayer, K. Hirai, and S. Blügel, Phys. Rev. Lett. **86**, 1106 (2001).

[13] H. Kobayashi, I. Tsujikawa, and I. Kimura, J. Phys. Soc. Jpn. **24**, 1169 (1968).

[14] E. Müller-Hartmann, U. Köbler, and L. Smardz, J. Magn. Magn. Mater. **173**, 133 (1997).

[15] S. Paul, S. Haldar, S. von Malottki, and S. Heinze, Nat. Commun. **11**, 1 (2020).

[16] M. Gutzeit, S. Haldar, S. Meyer, and S. Heinze, Phys. Rev. B **104**, 024420 (2021).

[17] J. Spethmann, S. Meyer, K. von Bergmann, R. Wiesendanger, S. Heinze, and A. Kubetzka, Phys. Rev. Lett. **124**, 227203 (2020).

[18] M. dos Santos Dias, S. Brinker, A. Lászlóffy, B. Nyári, S. Blügel, L. Szunyogh, and S. Lounis, Phys. Rev. B **103**, L140408 (2021).

[19] B. Hardrat, A. Al-Zubi, P. Ferriani, S. Blügel, G. Bihlmayer, and S. Heinze, Phys. Rev. B **79**, 094411 (2009).

[20] A. Al-Zubi, G. Bihlmayer, and S. Blügel, Phys. Status Solidi B **248**, 2242 (2011).

[21] S. Mankovsky, S. Polesya, and H. Ebert, Phys. Rev. B **101**, 174401 (2020).

[22] E. Harris and J. Owen, Phys. Rev. Lett. **11**, 9 (1963).

[23] D. Rodbell, I. Jacobs, J. Owen, and E. Harris, Phys. Rev. Lett. **11**, 10 (1963).

[24] B. D. Gaulin and M. F. Collins, Phys. Rev. B **33**, 6287 (1986).

[25] S. Bhattacharjee, V. B. Shenoy, and T. Senthil, Phys. Rev. B **74**, 092406 (2006).

[26] J. Lou, T. Xiang, and Z. Su, Phys. Rev. Lett. **85**, 2380 (2000).

[27] R. Bursill, T. Xiang, and G. Gehring, J. Phys. A: Math. Gen. **28**, 2109 (1995).

[28] A. Läuchli, G. Schmid, and S. Trebst, Phys. Rev. B **74**, 144426 (2006).

[29] G. De Chiara, M. Lewenstein, and A. Sanpera, Phys. Rev. B **84**, 054451 (2011).

[30] O. Mryasov, A. J. Freeman, and A. Liechtenstein, J. Appl. Phys. **79**, 4805 (1996).

[31] S. Heinze, K. Von Bergmann, M. Menzel, J. Brede, A. Kubetzka, R. Wiesendanger, G. Bihlmayer, and S. Blügel, Nat. Phys. **7**, 713 (2011).

[32] F. Michaud, F. Vernay, S. R. Manmana, and F. Mila, Phys. Rev. Lett. **108**, 127202 (2012).

[33] M. Hoffmann, J. Weischenberg, B. Dupé, F. Freimuth, P. Ferriani, Y. Mokrousov, and S. Heinze, Phys. Rev. B **92**, 020401(R) (2015).

[34] N. Romming, H. Pralow, A. Kubetzka, M. Hoffmann, S. von Malottki, S. Meyer, B. Dupé, R. Wiesendanger, K. von Bergmann, and S. Heinze, Phys. Rev. Lett. **120**, 207201 (2018).
[35] A. Krönlein, M. Schmitt, M. Hoffmann, J. Kemmer, N. Seubert, M. Vogt, J. Küspert, M. Böhme, B. Alonazi, J. Kügel *et al.*, Phys. Rev. Lett. **120**, 207202 (2018).
[36] R. Drautz and M. Fähnle, Phys. Rev. B **72**, 212405 (2005).
[37] M. Takahashi, J. Phys. C: Solid State Phys. **10**, 1289 (1977).
[38] A. H. MacDonald, S. M. Girvin, and D. Yoshioka, Phys. Rev. B **37**, 9753 (1988).
[39] M. Hoffmann and S. Blügel, Phys. Rev. B **101**, 024418 (2020).
[40] W. Li, S. Paul, K. von Bergmann, S. Heinze, and R. Wiesendanger, Phys. Rev. Lett. **125**, 227205 (2020).
[41] F. Michaud and F. Mila, Phys. Rev. B **88**, 094435 (2013).
[42] N. Chepiga, I. Affleck, and F. Mila, Phys. Rev. B **93**, 241108(R) (2016).
[43] N. Chepiga, I. Affleck, and F. Mila, Phys. Rev. B **94**, 205112 (2016).
[44] L. Vanderstraeten, E. Wybo, N. Chepiga, F. Verstraete, and F. Mila, Phys. Rev. B **101**, 115138 (2020).
[45] N. Chepiga, I. Affleck, and F. Mila, Phys. Rev. B **101**, 174407 (2020).
[46] Z.-Y. Wang, S. C. Furuya, M. Nakamura, and R. Komakura, Phys. Rev. B **88**, 224419 (2013).
[47] S. Brehmer, H.-J. Mikeska, and S. Yamamoto, J. Phys.: Condens. Matter **9**, 3921 (1997).
[48] S. Yamamoto, S. Brehmer, and H.-J. Mikeska, Phys. Rev. B **57**, 13610 (1998).
[49] S. Yamamoto, T. Fukui, and T. Sakai, Eur. Phys. J. B **15**, 211 (2000).
[50] A. E. Trumper and C. Gazza, Phys. Rev. B **64**, 134408 (2001).
[51] J. Abouie and A. Langari, Phys. Rev. B **70**, 184416 (2004).
[52] J. Abouie, S. A. Ghasemi, and A. Langari, Phys. Rev. B **73**, 014411 (2006).
[53] A. Langari, J. Abouie, M. Asadzadeh, and M. Rezai, J. Stat. Mech. (2011) P08001.
[54] N. B. Ivanov, J. Richter, and U. Schollwöck, Phys. Rev. B **58**, 14456 (1998).
[55] N. B. Ivanov, J. Ummethum, and J. Schnack, Eur. Phys. J. B **87**, 226 (2014).
[56] N. Ivanov and J. Schnack, in *Journal of Physics: Conference Series* (IOP Publishing, Varna, Bulgaria, 2014), Vol. 558, p. 012015.
[57] N. B. Ivanov, S. I. Petrova, and J. Schnack, Eur. Phys. J. B **89**, 121 (2016).
[58] N. Ivanov and J. Schnack, in *Journal of Physics: Conference Series* (IOP Publishing, Varna, Bulgaria, 2019), Vol. 1186, p. 012014.
[59] M. B. Hastings, J. Stat. Mech. (2007) P08024.
[60] J. Eisert, M. Cramer, and M. B. Plenio, Rev. Mod. Phys. **82**, 277 (2010).
[61] J. Colpa, Physica A **93**, 327 (1978).
[62] J. Colpa, Physica A **134**, 377 (1986).
[63] J. Colpa, Physica A **134**, 417 (1986).
[64] F. Heydarinasab and J. Abouie, Sci. Rep. **8**, 7955 (2018).
[65] F. Heydarinasab and J. Abouie, Phys. Rev. B **96**, 104406 (2017).
[66] J. Richter, O. Krupnitska, V. Baliha, T. Krokhmalskii, and O. Derzhko, Phys. Rev. B **97**, 024405 (2018).
[67] J. Schnack, J. Schulenburg, A. Honecker, and J. Richter, Phys. Rev. Lett. **125**, 117207 (2020).
[68] O. Derzhko, J. Richter, and M. Maksymenko, Int. J. Mod. Phys. B **29**, 1530007 (2015).
[69] T. M. Rice, Science **298**, 760 (2002).
[70] D. Yamamoto, A. Masaki, and I. Danshita, Phys. Rev. B **86**, 054516 (2012).
[71] D. Yamamoto, I. Danshita, and C. A. R. Sade Melo, Phys. Rev. A **85**, 021601(R) (2012).
[72] D. Yamamoto, Phys. Rev. B **79**, 144427 (2009).
[73] F. Heydarinasab and J. Abouie, J. Phys.: Condens. Matter **32**, 165804 (2020).
[74] A. Läuchli, F. Mila, and K. Penc, Phys. Rev. Lett. **97**, 087205 (2006).
[75] H.-H. Zhao, C. Xu, Q. N. Chen, Z. C. Wei, M. P. Qin, G. M. Zhang, and T. Xiang, Phys. Rev. B **85**, 134416 (2012).
[76] W.-J. Hu, S.-S. Gong, H.-H. Lai, Q. Si, and E. Dagotto, Phys. Rev. B **101**, 014421 (2020).
[77] O. Benton, L. D. C. Jaubert, R. R. P. Singh, J. Oitmaa, and N. Shannon, Phys. Rev. Lett. **121**, 067201 (2018).
[78] S. X. M. Riberolles, T. J. Slade, D. L. Abernathy, G. E. Granroth, B. Li, Y. Lee, P. C. Canfield, B. G. Ueland, L. Ke, and R. J. McQueeney, Phys. Rev. X **12**, 021043 (2022).